

Regularization by Texts for Latent Diffusion Inverse Solvers

Jeongsol Kim^{1*} Geon Yeong Park^{1*} Hyungjin Chung¹ Jong Chul Ye²
¹Dept. of Bio & Brain Engineering, ²Kim Jae Chul Graduate School of AI,
 KAIST

{jeongsol, pky3436, hj.chung, jong.ye}@kaist.ac.kr

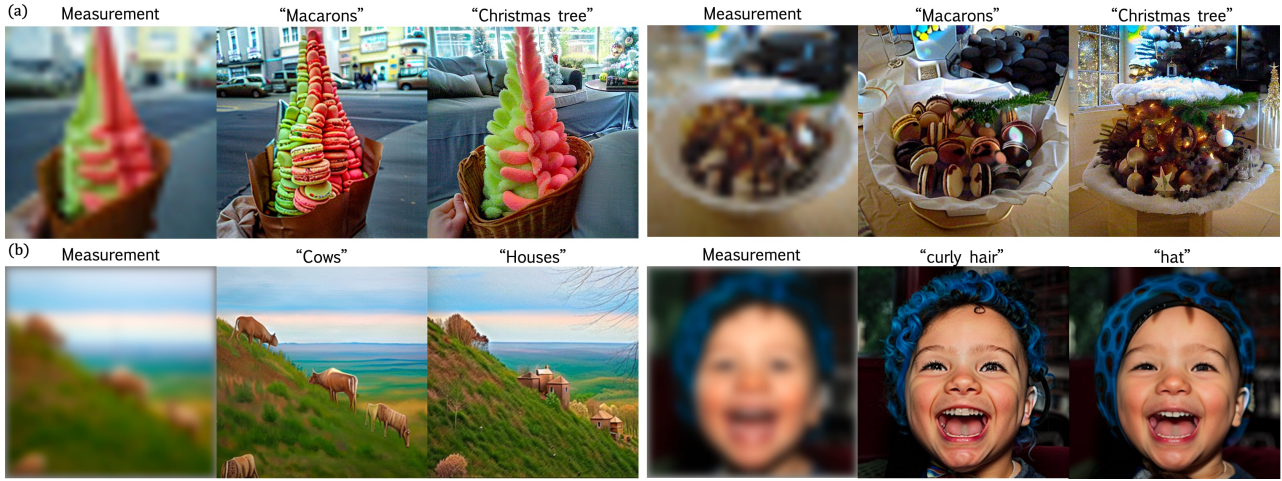


Figure 1. (a) Representative results for super-resolution (x16) with text-driven regularization. (b) Representative results for Gaussian deblurring task. Note that images are reconstructed according to given text prompt while it preserves the data consistency with given measurement.

Abstract

The recent advent of diffusion models has led to significant progress in solving inverse problems, leveraging these models as effective generative priors. Nonetheless, challenges related to the ill-posed nature of such problems remain, often due to inherent ambiguities in measurements. Drawing inspiration from the human ability to resolve visual ambiguities through perceptual biases, here we introduce a novel latent diffusion inverse solver by incorporating regularization by texts (TReg). Specifically, TReg applies the textual description of the preconception of the solution during the reverse sampling phase, of which description is dynamically reinforced through null-text optimization for adaptive negation. Our comprehensive experimental results demonstrate that TReg successfully mitigates ambiguity in latent diffusion inverse solvers, enhancing their effectiveness and accuracy.

1. Introduction

Consider the famous Rubin’s vase illusion, an optical illusion composed of a straightforward black and white image. This image can be perceived in two distinct ways: as a vase or as two faces in profile, facing each other. The interpretation hinges on the viewer’s perceptual bias, highlighting how human observation can vary dramatically in response to visual ambiguity.

Perceptual bias plays a crucial role in how we perceive and understand the world around us, especially in situations where visual information is incomplete, ambiguous, or open to multiple interpretations.

In fact, the process of visual perception can be interpreted as an inverse problem. Specifically, consider a given forward measurement process:

$$\mathbf{y} = \mathcal{A}(\mathbf{x}) + \epsilon \quad (1)$$

where $\mathcal{A} : \mathbb{R}^m \mapsto \mathbb{R}^m$ describes imaging systems, $\mathbf{y} \in \mathbb{R}^n$ and $\mathbf{x} \in \mathbb{R}^m$ represents the measurement and the true im-

age, respectively, and $\epsilon \in \mathbb{R}^n$ denotes the measurement noise. Then, an inverse solver attempts to recover \mathbf{x} from the measurement \mathbf{y} . Unfortunately, the majority of the inverse problems is ill-posed, implying that many different visual inputs produce the same measurements as significant amount of visual information in the original input is lost during the measurement process. Therefore, a naive application of the inverse solver leads to the ambiguity of the solutions. Classically, the regularization techniques have been extensively studied to address the ambiguity. For example, sparsity (L_1 norm), total variation (TV), and regularization by denoising (RED) have been widely used for regularization by exploiting the statistical properties of natural images [4, 26, 36]. Recently, with the advent of the diffusion model, new family of Diffusion Inverse Solvers (DIS) [6, 18, 24, 37] have been proposed with superior reconstruction performance. The main idea is to leverage the power of the diffusion model that has learned the score function of prior distribution to reduce the ill-posedness of the inverse problem.

While diffusion models have made substantial progress, it is important to note the persistent disparity between human perception and diffusion inverse solvers (DIS). For instance, confirmation bias in humans—where visual information is interpreted to align with pre-existing beliefs—plays a crucial and sometimes adverse role in resolving visual ambiguities. However, no equivalent mechanism in DIS currently applies these preconceptions during reconstruction. Furthermore, although the perceptual bias can be seen negatively due to the term ‘bias’, it can be often beneficial in many practical scenarios. For instance, in radiology, non-visual data such as lab results or clinical notes can be instrumental in clarifying the ambiguities inherent in imaging measurements.

To bridge the gap between human perception and diffusion inverse solvers (DIS), here we introduce a new concept: *Regularization by Text (TReg)* utilizing latent diffusion models. TReg specifically employs textual descriptions reflecting the preconceived notion of the desired outcome during the reverse sampling phase. However, a straightforward application of a text prompt reflecting these preconceptions is inadequate, as the intermediate images from reverse samples vary in noise levels. To effectively integrate the textual form of the preconception and guide the reverse sampling, we propose an innovative method of null text optimization for adaptive negation throughout the reverse sampling process. This approach dynamically adjusts the influence of the textual guide, ensuring it aligns with the evolving state of the reverse sampling.

Experimental results demonstrate that our method can effectively solve the linear inverse problems for a 512x512 size of image within 20 secs, while reducing the uncertainty and improving accuracy (Figure 1).

2. Background

Latent diffusion model. Image diffusion models that operate on the pixel space are compute-heavy. The latent diffusion model (LDM) [27] is a class of diffusion-based generative models [17, 30, 34], where the diffusion process is operated on latent space instead of the pixel space. Specifically, the LDM leverages a variational autoencoder that maximizes the evidence lower bound (ELBO) [19, 27]. This leads to the following latent representation:

$$\mathbf{z} = \mathcal{E}_\phi(\mathbf{x}) := \mathcal{E}_\phi^\mu(\mathbf{x}) + \mathcal{E}_\phi^\sigma(\mathbf{x}) \odot \epsilon, \quad \epsilon \sim \mathcal{N}(0, \mathbf{I}), \quad (2)$$

where \odot denotes the element-by-element multiplication, and $\mathcal{E}_\phi^\mu, \mathcal{E}_\phi^\sigma$ are parts of the encoder that outputs the mean and the variance of the encoder distribution. The resulting pixel domain representation can be obtained by

$$\mathbf{x} = \mathcal{D}_\varphi(\mathbf{z}) \quad (3)$$

where \mathcal{D}_φ is the decoder.

Then, the forward diffusion starts from the the latent representation for the clean image $\mathbf{z}_0 = \mathcal{E}(\mathbf{x}) \in \mathbb{R}^d$ and generates samples $\mathbf{z}_t = \sqrt{\bar{\alpha}_t}\mathbf{z}_0 + \sqrt{1 - \bar{\alpha}_t}\epsilon$ using VP-SDE formulation. Accordingly, the neural backbone $\epsilon_\theta(\cdot, t)$ is trained to estimate the noise ϵ from \mathbf{z}_t by solving the following optimization problem:

$$\min_{\theta} \mathbb{E}_{\mathcal{E}(\mathbf{x}), \epsilon \sim \mathcal{N}(0, \mathbf{I}), t} [\|\epsilon - \epsilon_\theta(\mathbf{z}_t, t)\|_2^2], \quad (4)$$

where the neural network ϵ_θ is commonly selected as time-conditional UNet [28]. Notably, the optimal solution ϵ_θ^* of (4) can be used to derive a score function as $\nabla_{\mathbf{z}_t} \log p(\mathbf{z}_t) = -\epsilon_\theta^*(\mathbf{z}_t, t)/\sqrt{1 - \bar{\alpha}_t}$ [34]. After training, we can conduct the reverse sampling from $p_\theta(\mathbf{z}_{t-1}|\mathbf{z}_t)$ as

$$\hat{\mathbf{z}}_0 = \mathbb{E}[\mathbf{z}_0|\mathbf{z}_t] = (\mathbf{z}_t - \sqrt{1 - \bar{\alpha}_t}\epsilon_\theta(\mathbf{z}_t, t))/\sqrt{\bar{\alpha}_t} \quad (5)$$

$$\mathbf{z}_{t-1} = \sqrt{\bar{\alpha}_{t-1}}\hat{\mathbf{z}}_0 + \sqrt{1 - \bar{\alpha}_{t-1}}\epsilon_\theta(\mathbf{z}_t, t), \quad (6)$$

under the assumption of deterministic DDIM sampling [32].

Classifier Free Guidance. By inheriting the classifier guidance of generative models, [13] has proposed the classifier guidance for deterministic DDIM sampling by defining epsilon prediction that corresponds to $\nabla_{\mathbf{z}_t} \log p(\mathbf{z}_t|\mathbf{c})$,

$$\hat{\epsilon}_\theta = \epsilon_\theta(\mathbf{z}_t, t) - \omega\sqrt{1 - \bar{\alpha}_t}\nabla_{\mathbf{z}_t} \log p(\mathbf{c}|\mathbf{z}_t) \quad (7)$$

where ω is a scale ¹ for the guidance and $\nabla_{\mathbf{z}_t} \log p(\mathbf{c}|\mathbf{z}_t)$ is computed by a trained classifier. Thus, it requires additional classifier training on noisy dataset which exhibits expensive computational cost. Furthermore, to reduce additional computation costs from classifier training, [16] proposed the

¹If $\omega = 1.0$, $\hat{\epsilon}_\theta = \sqrt{1 - \bar{\alpha}_t}\nabla_{\mathbf{z}_t} \log p(\mathbf{z}_t|\mathbf{c})$. Otherwise, we are approximating $p(\mathbf{z}_t|\mathbf{c}) \propto p(\mathbf{z}_t|\mathbf{c})p(\mathbf{c}|\mathbf{z}_t)^\omega$

classifier-free-guidance by substituting $\nabla_{\mathbf{z}_t} \log p(\mathbf{c}|\mathbf{z}_t) = \nabla_{\mathbf{z}_t} \log p(\mathbf{z}_t|\mathbf{c}) - \nabla_{\mathbf{z}_t} \log p(\mathbf{z}_t)$ so that the epsilon prediction is defined as

$$\hat{\epsilon}_\theta = \epsilon_\theta(\mathbf{z}, \phi, t) + \omega(\epsilon_\theta(\mathbf{z}, \mathbf{c}, t) - \epsilon_\theta(\mathbf{z}, \phi, t)), \quad (8)$$

where ϕ denotes *null-text* that indicates the class identifier for unconditional score prediction (i.e. $\epsilon_\theta(\mathbf{z}_t, t) = \epsilon_\theta(\mathbf{z}_t, \phi, t)$) to achieve both unconditional/conditional score prediction with a single neural network. It is noteworthy that the null-text token is also a learnable parameter of LDM.

Diffusion Inverse Solvers. Recently diffusion models have been extensively used as powerful generative priors for inverse problems [6, 9, 18, 24, 33, 37]. Earlier techniques in inverse imaging relied on an alternating projection method [5, 7, 34], enforcing hard measurement constraints between denoising steps in either pixel or measurement spaces. More advanced strategies have been proposed to approximate the gradient of the log posterior within diffusion models, broadening the scope to tackle nonlinear problems [6]. The field has seen further expansion with methods addressing blind inverse problem [8], 3D [10, 20], and problems of unlimited resolution [2]. Traditionally, these methods have utilized image-domain diffusion models, but a shift has been observed towards latent diffusion models such as latent DPS (LDPS) with fixed point of autoencoder process [29], LDPS with history update [14] and Resample [31]. Despite these innovations, the use of text embedding for regularization is often overlooked, which we opt to address.

3. Main Contribution: Regularization by Text

In this section, we provide a mathematical derivation of our reverse sampling step. Specifically, the reverse sampling consists of three distinct steps: 1) adaptive negation for reinforcing the textual constraint, 2) latent optimization to impose measurement and latent space consistency, and 3) DDPM type forward sampling to return the intermediate reconstruction to correct noisy manifold. The details are as follows.

3.1. Adaptive negation for textual constraint

While the text prompt for LDM can effectively narrow down the solution space, directly employing text prompts via CFG may not adequately capture the intended guidance due to the inherent error-prone nature of hand-crafted prompts. In other words, the provided text prompts may not represent the optimal conditioning.

To resolve this, one can leverage the prompt tuning [21], but it can disrupt the user intention included in the text prompt during the tuning process. Intriguingly, instead of

finding an optimal text prompt that matches the user intention, we found that the concept negation [16] that comprises complement concepts of the given text prompt is effective to reinforce the original user’s concept.

Specifically, with the aid of the CFG, leveraging the null-text token facilitates the concept negation and the suppression of the complement concept is achievable by optimizing the null-text token. In particular, during the reverse sampling, we minimize the following cost function on the CLIP [25] embedding space:

$$\mathcal{L}_\phi = \text{sim}(\mathcal{T}_{img}(\hat{\mathbf{x}}_0(\mathbf{y})), c_\phi), \quad (9)$$

where c_ϕ is the embedded null-text token via CLIP text encoder, \mathcal{T}_{img} denotes CLIP image encoder, $\hat{\mathbf{x}}_0(\mathbf{y})$ denotes denoised estimates on pixel space which is updated by the data consistency, and $\text{sim}(\cdot, \cdot)$ denotes inner product.

By minimizing the similarity between intermediate images $\hat{\mathbf{x}}_0$ and the null-text in the CLIP space, we can make the null-text to have complementary concepts for given contexts which is accumulated to the intermediate images $\hat{\mathbf{x}}_0$. This approach considers only the null-text token as a variable, and since back-propagation to other neural networks does not occur, the computational cost is negligible. This makes the proposed method extremely cost-effective for enhancing text guidance.

3.2. Latent Optimization

For the latent optimization, consider the following loss, which is the maximum a posteriori (MAP) objective under the VAE prior in (2) by assuming that $\mathcal{E}_\phi^\sigma(\mathbf{x})$ is isotropic, i.e. $\mathcal{E}_\phi^\sigma(\mathbf{x}) = \sigma_\epsilon \mathbf{1}$:

$$\mathcal{L}(\mathbf{x}, \mathbf{z}) = \frac{\|\mathbf{y} - \mathcal{A}(\mathcal{D}_\varphi(\mathbf{z}))\|_2^2}{2\sigma^2} + \frac{\|\mathbf{z} - \mathcal{E}_\phi^\mu(\mathbf{x})\|_2^2}{2\sigma_\epsilon^2}. \quad (10)$$

We can now minimize (10) using the proximal optimization. Specifically, for an initial latent $\mathbf{z}_0 := \hat{\mathbf{z}}_{0|t}$ from the Tweedie’s formula, the proximal approach compute the solution that minimizes the following:

$$\mathcal{L}(\mathbf{x}, \mathbf{z}) + \gamma \|\mathbf{z} - \mathbf{z}_0\|^2 \quad (11)$$

which we are interested in solving by variable splitting similar in spirit to the alternating direction method of multipliers [4]. Namely, using the decoder approximation and setting $\mathbf{x} = \mathcal{D}_\varphi^\mu(\mathbf{z})$, the optimization problem with respect to \mathbf{x} and becomes

$$\min_{\mathbf{x}} \frac{\|\mathbf{y} - \mathcal{A}(\mathbf{x})\|_2^2}{2\sigma^2} + \frac{\|\mathbf{z} - \mathcal{E}_\phi^\mu(\mathbf{x})\|_2^2}{2\sigma_\epsilon^2} + \lambda \|\mathbf{x} - \mathcal{D}_\varphi(\mathbf{z}) + \boldsymbol{\eta}\|_2^2. \quad (12)$$

Here, for simplicity, we set dual variable $\boldsymbol{\eta}$ as a zero vector and do not consider its update. Then, from the initialization

with $z = z_0$, we have

$$\hat{x}_0(\mathbf{y}) = \arg \min_{\mathbf{x}} \frac{\|\mathbf{y} - \mathcal{A}(\mathbf{x})\|_2^2}{2\sigma^2} + \lambda \|\mathbf{x} - \mathcal{D}_\varphi(\hat{z}_{0|t})\|_2^2, \quad (13)$$

which can be solved with negligible computation cost such as conjugate gradient (CG). Subsequently, using the encoder approximation and setting $z = \mathcal{E}_\phi(\mathbf{x})$ with $\boldsymbol{\eta} = \mathbf{0}$, the optimization problem with respect to z reads

$$\hat{z}_0^{ema} = \arg \min_z \zeta \|z - \hat{z}_0(\mathbf{y})\|_2^2 + \gamma \|z - \hat{z}_0(z_t)\|_2^2 \quad (14)$$

where $\hat{z}_0(\mathbf{y}) := \mathcal{E}_\phi(\hat{x}_0(\mathbf{y}))$, leading to a closed-form solution

$$\hat{z}_0^{ema} = \bar{\alpha}_{t-1} \hat{z}_0(\mathbf{y}) + (1 - \bar{\alpha}_{t-1}) \hat{z}_0(z_t) \quad (15)$$

where ζ, γ are chosen to satisfy $\bar{\alpha}_{t-1} = \zeta / (\zeta + \gamma)$.

3.3. DDIM Sampling

The general form of the update rule of the DDIM [32] is given as follows

$$z'_{t-1} = \sqrt{\bar{\alpha}_{t-1}} \hat{z}_0 + \sqrt{1 - \bar{\alpha}_{t-1}} \tilde{\epsilon}_t \quad (16)$$

where \hat{z}_0 is the *denoised* estimate and $\tilde{\epsilon}_t$ denotes the total noise given by

$$\tilde{\epsilon}_t := \frac{\sqrt{1 - \bar{\alpha}_{t-1} - \eta^2 \tilde{\beta}_t^2} \hat{\epsilon}_\theta + \eta \tilde{\beta}_t \epsilon}{\sqrt{1 - \bar{\alpha}_{t-1}}} \quad (17)$$

In (16), $\eta \in [0, 1]$ is a parameter controlling the stochasticity of the update rule: $\eta = 0.0$ leads to fully deterministic sampling, whereas $\eta = 1.0$ with $\tilde{\beta}_t = \sqrt{(1 - \bar{\alpha}_{t-1}) / (1 - \bar{\alpha}_t)} \sqrt{1 - \bar{\alpha}_t / \bar{\alpha}_{t-1}}$ recovers the ancestral sampling of DDPMs.

3.4. Latent DPS

Plugging in $\hat{z}_{0|t}$ from the Tweedie's formula, we can obtain the standard LDPS gradient equipped with \hat{c}_θ , the optimized null text embedding

$$z_{t-1} = z'_{t-1} - \rho_t \nabla_{z_t} \|\mathcal{A}(\mathcal{D}_\varphi(\hat{z}_{0|t}, \hat{c}_\theta)) - \mathbf{y}\| \quad (18)$$

where we set ρ_t to be the step size that weights the likelihood, similar to [6]. Due to the computational complexity of DPS, we often neglect the DPS update term for computational saving. Nevertheless, our algorithm can effectively solve the problem and shows comparable performance with DPS update as shown in Figure 2.

To sum up, the proposed algorithm is described as in Algorithm 1.

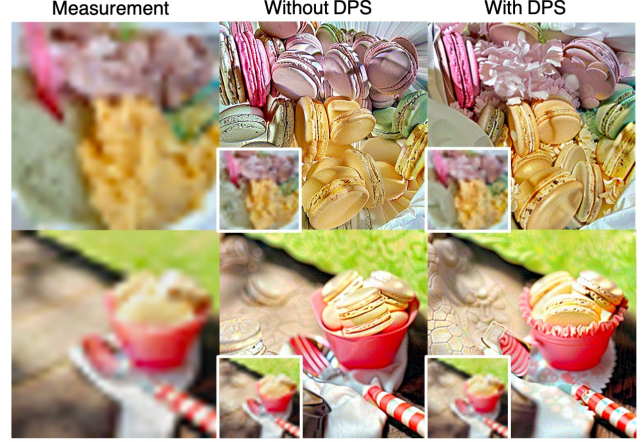


Figure 2. Comparison with and without DPS update. Measurements are generated by SR (x16). Down-sampled images are displayed as insets. Class : "ice cream". Prompt "macaron".

Algorithm 1 Inverse problem solving with TReg

Require: $\epsilon_\theta, \phi, c, \mathcal{E}, \mathcal{D}, \mathcal{A}, y, \mathcal{T}_{img}$

$z_T \sim \mathcal{N}(0, \mathbf{I})$

for $t \in [T, 1]$ **do**

$\hat{\epsilon}_\theta = \epsilon_\theta(z_t, \phi) + \omega(\epsilon_\theta(z_t, c) - \epsilon_\theta(z_t, \phi))$

$\hat{z}_{0|t} = (z_t - \sqrt{1 - \bar{\alpha}_t} \hat{\epsilon}_\theta) / \sqrt{\bar{\alpha}_t}$

if $t \in \Gamma$ **then**

$\hat{x}_0 \leftarrow \mathcal{D}(\hat{z}_{0|t})$

$\hat{x}_0(\mathbf{y}) \leftarrow \arg \min_{\mathbf{x}} \frac{\|\mathbf{y} - \mathcal{A}(\mathbf{x})\|_2^2}{2\sigma^2} + \lambda \|\mathbf{x} - \hat{x}_0\|_2^2$

$\hat{z}_0(\mathbf{y}) \leftarrow \mathcal{E}(\hat{x}_0(\mathbf{y}))$

$\hat{c}_\theta \leftarrow c_\theta - \eta \nabla_\phi(\text{sim}(\mathcal{T}_{img}(\hat{x}_0(\mathbf{y})), c_\theta))$

$\hat{z}_0^{ema} \leftarrow \bar{\alpha}_{t-1} \hat{z}_0(\mathbf{y}) + (1 - \bar{\alpha}_{t-1}) \hat{z}_0(z_t)$

$\tilde{\epsilon}_t \leftarrow \frac{\sqrt{1 - \bar{\alpha}_{t-1} - \eta^2 \tilde{\beta}_t^2} \hat{\epsilon}_\theta + \eta \tilde{\beta}_t \epsilon}{\sqrt{1 - \bar{\alpha}_{t-1}}}$ State

$z'_{t-1} \leftarrow \sqrt{\bar{\alpha}_{t-1}} \hat{z}_0^{ema} + \sqrt{1 - \bar{\alpha}_{t-1}} \tilde{\epsilon}_t$

else

$z'_{t-1} \leftarrow \sqrt{\bar{\alpha}_{t-1}} \hat{z}_0(z_t) + \sqrt{1 - \bar{\alpha}_{t-1}} \tilde{\epsilon}_t$

end if

$z_{t-1} \leftarrow z'_{t-1} - \rho_t \nabla_{z_t} \|\mathcal{A}(\mathcal{D}_\varphi(\hat{z}_{0|t}, \hat{c}_\theta)) - \mathbf{y}\|$

end for

4. Experiments

4.1. Experimental settings

Forward models In this study, we utilize more extreme forward operations than those used in previous works to ensure a sufficient null-space. Specifically, we use the bicubic downsampling with scale factor 16, Gaussian blurring with kernel size 61 and sigma 5.0 as our forward operations. We define the linear forward operations and its transpose by following the previous studies [9, 18, 33, 37]. For the measurement noise, we use the noise scale $\sigma_0^2 = 0.01$ for all tasks.

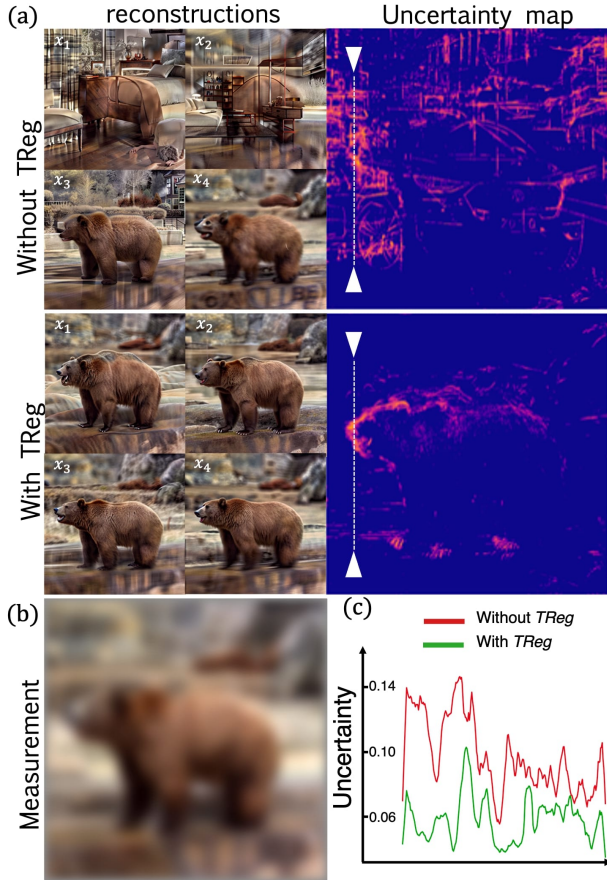


Figure 3. TReg reduces the ambiguity. Given text prompt for TReg is "bear". (a) Reconstructions and uncertainty map (b) Measurement is generated by Gaussian blur. (c) Uncertainty value across white dotted lines on (a). Gaussian smoothing with kernel width 10 pixels is applied for visualization.

Baselines As the first attempt to solve inverse problem using text-driven regularization, we establish baselines by combining 1) data consistency-preserving methods and 2) text-guided editing methods. Notably, these baselines involve sequential processing, while the proposed method stands out for its efficiency, eliminating the need for pre/post-hoc techniques. For data consistency methods, we utilize the measurement itself and PSLD [29] which is a LDM-based inverse problem solver. Regarding text-guided editing methods, we opt for state-of-the-art techniques, namely Delta Denoising Score (DDS) [15] and Plug-and-Play diffusion (PnP) [35]. Since PnP involves inversion process, we handle it as two stages approach. Also, we use PSLD with text guidance as our baseline to examine the incompatibility between the data consistency and CFG in its current form.

Dataset and text prompt For the effective quantitative evaluation, it is crucial to select the measurement and text prompt that do not conflict each other. This ensures that the generated features through textual guidance coherently maintain the data consistency across the entire dataset. Furthermore, selecting an improper text prompt c (for instance, "dog" for the measurement generated by baby image) can lead to undesired outcomes such as ignoring the provided guidance. After exploring various datasets, we have determined that Food-101 dataset [3] is well-suited for our quantitative comparison due to its non-sparse and complex patterns. Also, given that all images in this dataset fall under the 'food' category, it becomes more straightforward to select an appropriate c aligned with the original caption. Specifically, we leverage 250 images from each of the "fried rice" and "ice cream" classes, accompanied by the corresponding text prompts "spaghetti" and "macarons". Also, we design the null-text update schedule since the reconstructed images become saturated and fidelity is decreased if the null-text is optimized too frequently. Therefore, we apply updates to the null-text only when data consistency updates are performed. For the optimization, we use AdamW [22] optimizer with learning rate $1e-3$ and update null-text for 10 iterations per time step. For the qualitative comparison, we additionally use validation set of ImageNet [12].

4.2. Experimental Results

Ambiguity reduction In this section, an experimental analysis is conducted to assess the efficacy of TReg in mitigating uncertainty inherent in inverse problems. Specifically, a comparative evaluation is performed between the proposed method with and without the TReg component. The elimination of TReg involves employing a null-text (\emptyset) as the text prompt while retaining adaptive negation, serving as an additional tool to suppress complementary concepts and enhance the generated image quality. Multiple iterations of the inverse problem are solved using 10 random seeds for a fixed super-resolution measurement.

The outcomes, depicted in Figure 3, consistently demonstrate that the TReg leads to intended solution corresponding to the given prompt. Conversely, in the absence of TReg, reconstructed images exhibit random artifacts, such as a car in the background or bedroom. This discrepancy is clearly observed in its uncertainty map in Figure 3 which is defined as pixel-wise standard deviation values, revealing heightened uncertainty levels without TReg, particularly in regions corresponding to distinct objects or characters. Although TReg implementation reduces uncertainty, some residual uncertainty persists, primarily attributed to in-class variations, notably in aspects like head positioning or mouth shape. However, it is noteworthy that these residual uncertainties does not violate the data consistency on

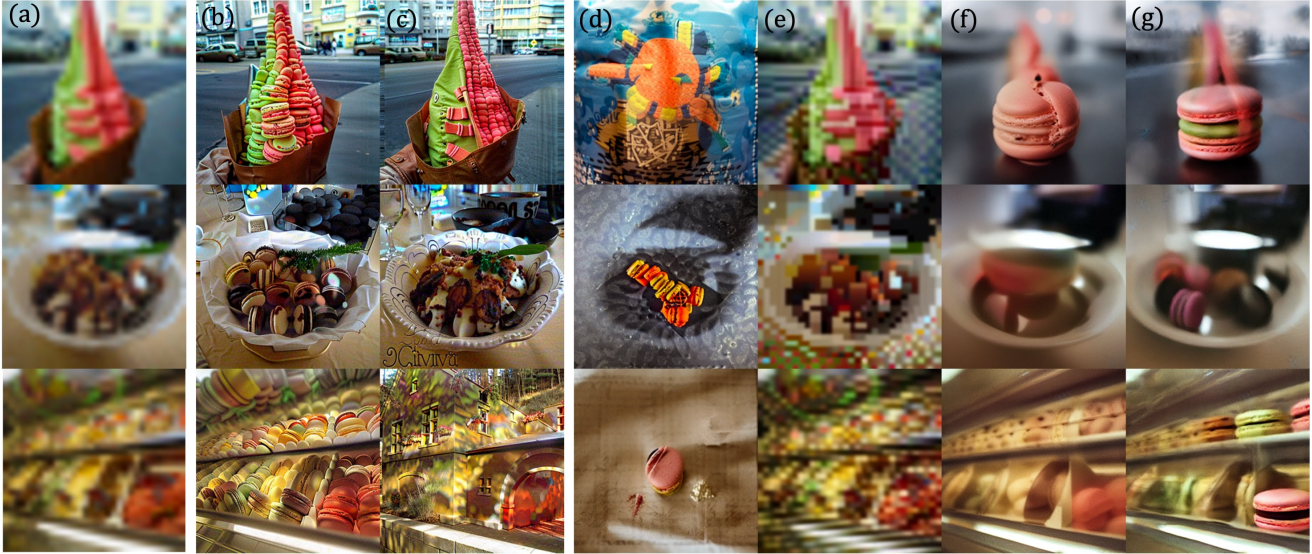


Figure 4. Representative reconstructed images for super-resolution (x16). Original class is "ice cream" and given prompt is "macaron". (a) Measurement (b) Ours **with** TReg (c) Ours **without** TReg (d) PSLD with text-guidance (e) PnP (f) PSLD + PnP (g) PSLD + DDS.

the measurement space.

Solving extreme inverse problems In this section, we conduct a quantitative comparison with baseline methods for super-resolution and deblur tasks. The evaluation is based on three metrics: LPIPS, the mean squared error between the provided measurement and the predicted measurement, namely $y\text{-MSE}^2$, and the CLIP similarity between the reconstructed image and the text prompt following the prior works in image editing [15, 35]. Each metric provides 1) quality of the reconstructed images, 2) data consistency, and 3) quality of text guidance, which allows us to investigate the advantage of TReg on inverse problems. Note that LPIPS is computed with respect to real images with class of target prompt.

Table 1 and 2 demonstrate the performance for the 16x super-resolution task and the Gaussian deblurring task, respectively. These results show that the proposed method gets a low LPIPS and $y\text{-MSE}$ which implies that the reconstructed image by LDM with TReg shows the high-quality while preserving data consistency at most. While PSLD attains remarkably low LPIPS scores in some tasks, such enhancements are not rooted in an inverse problem-solving process, as evidenced in abnormal $y\text{-MSE}$ and Figure 4d. Furthermore, for the CLIP similarity, the proposed method achieves comparable or better performance compared to state-of-the-art image editing algorithms, which supports the effectiveness of text guidance by the LDM with TReg.

Applying the editing algorithm directly to the measurement, denoted as PnP, exhibits sub-optimal performance

²In formula, we compute $\|y - \mathcal{A}x\|_2^2$.

# stages	method	Fired Rice \rightarrow Spaghetti			Ice Cream \rightarrow Macaron		
		LPIPS \downarrow	CLIP-sim \uparrow	$y\text{-MSE} \downarrow$	LPIPS \downarrow	CLIP-sim \uparrow	$y\text{-MSE} \downarrow$
1	Ours	0.769	0.303	0.005	<u>0.771</u>	<u>0.314</u>	0.004
	PSLD	0.756	0.265	0.020	0.743	0.293	0.020
2	PnP	0.826	0.251	0.005	0.808	0.239	<u>0.005</u>
	PSLD+DDS	0.788	0.247	<u>0.010</u>	<u>0.772</u>	0.328	0.013
3	PSLD+PnP	0.801	<u>0.291</u>	0.014	0.784	0.306	0.008

Table 1. Quantitative evaluation of SRx16 task. Mean values are reported. **Bold**: the best score, underline: the second best.

across all metrics except $y\text{-MSE}$ which indicates the inherent challenge of the problem that cannot be addressed without an inverse problem solver. Even for the case of $y\text{-MSE}$, it achieves a lower value since it does not make significant changes on measurement (column (e) in Figure 4 and 5).

This result implies that while text-guided image editing algorithms excel in reflecting the provided text prompt, they struggle to maintain data consistency with the given measurement. This points to the limitation of the sequential approach, where reconstruction errors accumulate at each stage, leading to substantial errors in the final outcome. In contrast, the proposed method effectively reflects the given text prompt while maintaining robust data consistency which supports the validity of the method.

Figure 4 and 5 presents a qualitative comparison between the proposed method and the baseline methods. The quality of the reconstructed image aligns with the quantitative results. Interestingly, PnP and DDS show a notable similarity in the direction of editing, with DDS tending to generate relatively sharper images. However, both methods compromise consistency with the given measurement. In contrast,

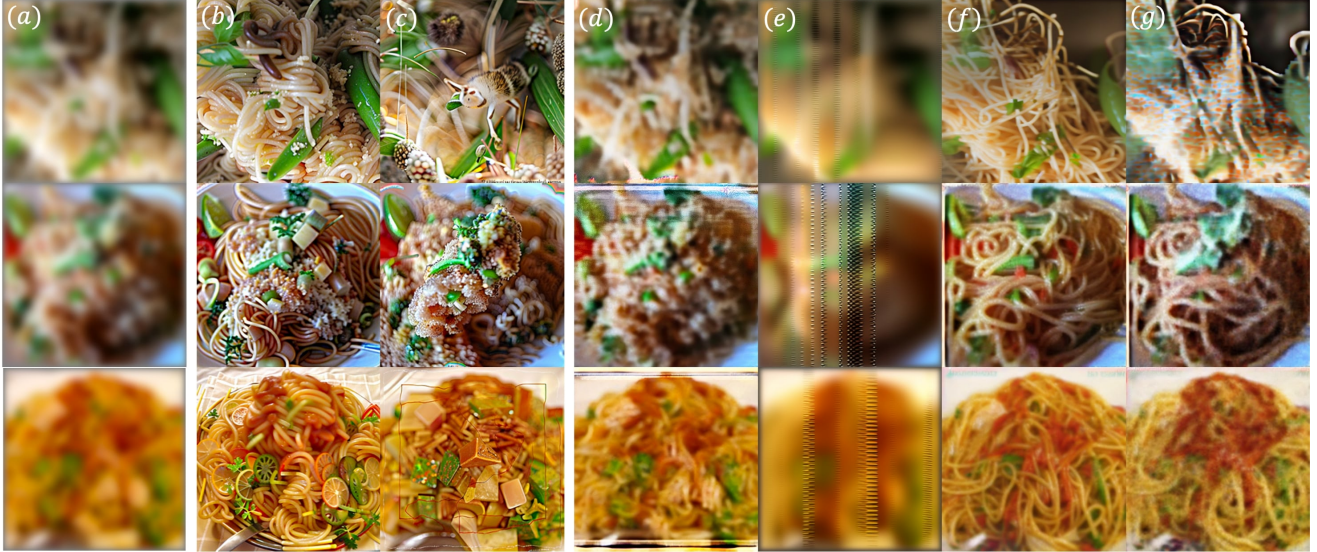


Figure 5. Representative reconstructed images for Gaussian deblurring. Original class is "fried rice" and given prompt is "spaghetti". (a) Measurement (b) Ours **with** TReg (c) Ours **without** TReg (d) PSLD with text-guidance (e) PnP (f) PSLD + PnP (g) PSLD + DDS

# stages	method	Fried Rice \rightarrow Spaghetti			Ice Cream \rightarrow Macaron		
		LPIPS \downarrow	CLIP-sim \uparrow	y-MSE \downarrow	LPIPS \downarrow	CLIP-sim \uparrow	y-MSE \downarrow
1	Ours	0.737	0.300	0.013	0.743	0.312	0.011
	PSLD	0.798	0.274	0.013	0.750	0.252	0.011
2	PnP	0.798	0.259	0.015	0.752	0.248	0.011
	PSLD+DDS	0.768	0.247	<u>0.014</u>	0.752	0.300	0.015
3	PSLD+PnP	<u>0.761</u>	0.312	0.016	<u>0.751</u>	0.319	<u>0.013</u>

Table 2. Quantitative evaluation of Gaussian deblur task. Mean values are reported. **Bold**: the best score, underline: the second best.

our method effectively preserves data consistency. Meanwhile, we also compare the results of our method without TReg and PSLD with CFG guidance. When TReg is removed from our method (column (c) in Figure 4 and 5), it provides a solution that aligns well with the given measurement but generates arbitrary structures. This result highlights the impact of TReg that reduces the ambiguity of inverse problem solving. PSLD with CFG guidance (column (d) in Figure 4 and 5) also fails to appropriately reflect given text prompt, as there is no consideration for text-guidance in solving inverse problems.

4.3. Increasing controllability with TReg

In previous sections, we demonstrate that text-driven regularization successfully mitigates the uncertainty of inverse problems and produces consistent reconstruction for a given measurement and a single text prompt, which is not enabled with all baseline methods. In this section, we investigate the capability of TReg to reconstruct the true signal based on multiple texts with a single identical measurement. Given

that the primary role of TReg is to diminish the solution space according to $p(z|c)$, the proposed method is expected to reconstruct diverse images in response to the provided text prompt. Figure 6 illustrates the results of solving inverse problems for SR and deblurring tasks with various text prompts. Regardless of the forward operation or data domain, the proposed method effectively reconstructs the solution. Importantly, different solutions maintain consistency with the given measurement. This distinctive feature sets our proposed approach apart from conventional stylization or personalization methods. Furthermore, the result directly shows the existence of multiple solutions that satisfied given forward model, which is an evidence of the ill-posedness nature of the inverse problem.

5. Related work

Leveraging text prompts for inverse problem solving has been studied in several recent works. TextIR [1] incorporates text embedding from CLIP during the training of an image restoration network to constrain the solution space in the case of extreme inverse problems. DA-CLIP [23] takes a similar approach of leveraging the embeddings and applies it to diffusion bridges. P2L [11] proposes to automatically tune text embedding on-the-fly while running a generic diffusion inverse problem solver. Notably, the latter two methods [11, 23] are focused on improving the overall performance rather than constraining the solution space. TextIR has similar objective to TReg, but requires task-specific training. In this regard, to the best of our knowledge, TReg is the first generic diffusion-based inverse problem solver that does not require task-specific training, while being able

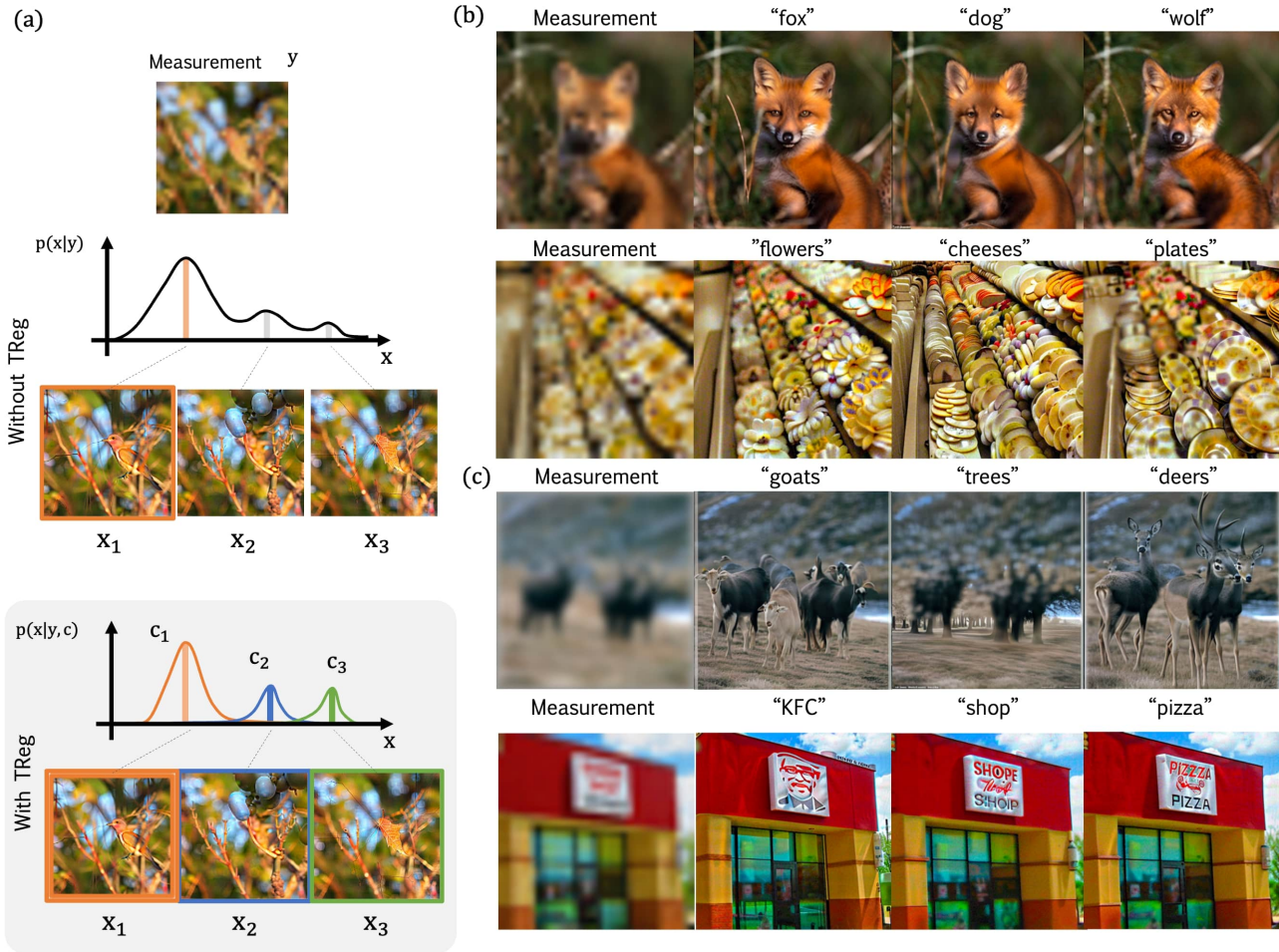


Figure 6. Additional results with multiple prompts. Measurements are generated by ImageNet validation set. (a) With $TReg$, we can solve the inverse problem with multiple prompts for a fixed measurement. (b) Super-resolution (c) Deblur (Gauss). Best views are displayed.

to incorporate text conditions to effectively control the solution space.

6. Conclusion

This study introduces a novel concept of latent diffusion inverse solver with *regularization by texts*, namely $TReg$. The proposed solver minimizes ambiguity in solving inverse problems, effectively reducing uncertainty and improving accuracy in visual reconstructions, bridging the gap between human perception and machine-based interpretation. To achieve this, we derive LDM-based reverse sampling steps to minimize data consistency with text-driven regularization, consisting of adaptive negation. Specifically, to effectively integrate textual cues and guide reverse sampling, the paper introduces a null text optimization approach. Experimental results and visualizations demonstrate that text-driven regularization effectively reduces the uncertainty of solving inverse problem, and further enables

text-guided control of signal reconstruction.

7. Potential negative impacts

In this study, the proposed text regularization is heavily influenced by prior. Therefore, if there is bias in a model utilized as a prior, such as in the case of stable diffusion, the solution to the inverse problem may also contain bias. As a restoration model controllable through text, there is a potential for misuse, such as the generation of fake news. Countermeasures should be established to prevent incorrect results and ensure the integrity of the outcomes.

References

- [1] Yunpeng Bai, Cairong Wang, Shuzhao Xie, Chao Dong, Chun Yuan, and Zhi Wang. Textir: A simple framework for text-based editable image restoration. *arXiv preprint arXiv:2302.14736*, 2023. 7
- [2] Sam Bond-Taylor and Chris G Willcocks. ∞ -diff: Infinite

- resolution diffusion with subsampled mollified states. *arXiv preprint arXiv:2303.18242*, 2023. 3
- [3] Lukas Bossard, Matthieu Guillaumin, and Luc Van Gool. Food-101 – mining discriminative components with random forests. In *European Conference on Computer Vision*, 2014. 5
- [4] Stephen Boyd, Neal Parikh, Eric Chu, Borja Peleato, Jonathan Eckstein, et al. Distributed optimization and statistical learning via the alternating direction method of multipliers. *Foundations and Trends® in Machine learning*, 3(1):1–122, 2011. 2, 3
- [5] Jooyoung Choi, Sungwon Kim, Yonghyun Jeong, Youngjune Gwon, and Sungroh Yoon. Ilvr: Conditioning method for denoising diffusion probabilistic models. *arXiv preprint arXiv:2108.02938*, 2021. 3
- [6] Hyungjin Chung, Jeongsol Kim, Michael T Mccann, Marc L Klasky, and Jong Chul Ye. Diffusion posterior sampling for general noisy inverse problems. *arXiv preprint arXiv:2209.14687*, 2022. 2, 3, 4
- [7] Hyungjin Chung, Byeongsu Sim, and Jong Chul Ye. Come-closer-diffuse-faster: Accelerating conditional diffusion models for inverse problems through stochastic contraction. In *Proceedings of the IEEE/CVF Conference on Computer Vision and Pattern Recognition*, pages 12413–12422, 2022. 3
- [8] Hyungjin Chung, Jeongsol Kim, Sehui Kim, and Jong Chul Ye. Parallel diffusion models of operator and image for blind inverse problems. In *Proceedings of the IEEE/CVF Conference on Computer Vision and Pattern Recognition*, pages 6059–6069, 2023. 3
- [9] Hyungjin Chung, Suhyeon Lee, and Jong Chul Ye. Fast diffusion sampler for inverse problems by geometric decomposition. *arXiv preprint arXiv:2303.05754*, 2023. 3, 4
- [10] Hyungjin Chung, Dohoon Ryu, Michael T McCann, Marc L Klasky, and Jong Chul Ye. Solving 3d inverse problems using pre-trained 2d diffusion models. In *Proceedings of the IEEE/CVF Conference on Computer Vision and Pattern Recognition*, pages 22542–22551, 2023. 3
- [11] Hyungjin Chung, Jong Chul Ye, Peyman Milanfar, and Mauricio Delbracio. Prompt-tuning latent diffusion models for inverse problems. *arXiv preprint arXiv:2310.01110*, 2023. 7
- [12] Jia Deng, Wei Dong, Richard Socher, Li-Jia Li, Kai Li, and Li Fei-Fei. Imagenet: A large-scale hierarchical image database. In *2009 IEEE conference on computer vision and pattern recognition*, pages 248–255. Ieee, 2009. 5
- [13] Prafulla Dhariwal and Alexander Nichol. Diffusion models beat gans on image synthesis. *Advances in neural information processing systems*, 34:8780–8794, 2021. 2
- [14] Linchao He, Hongyu Yan, Mengting Luo, Kunming Luo, Wang Wang, Wenchao Du, Hu Chen, Hongyu Yang, and Yi Zhang. Iterative reconstruction based on latent diffusion model for sparse data reconstruction. *arXiv preprint arXiv:2307.12070*, 2023. 3
- [15] Amir Hertz, Kfir Aberman, and Daniel Cohen-Or. Delta denoising score. In *Proceedings of the IEEE/CVF International Conference on Computer Vision*, pages 2328–2337, 2023. 5, 6
- [16] Jonathan Ho and Tim Salimans. Classifier-free diffusion guidance. *arXiv preprint arXiv:2207.12598*, 2022. 2, 3
- [17] Jonathan Ho, Ajay Jain, and Pieter Abbeel. Denoising diffusion probabilistic models. *Advances in neural information processing systems*, 33:6840–6851, 2020. 2
- [18] Bahjat Kawar, Michael Elad, Stefano Ermon, and Jiaming Song. Denoising diffusion restoration models. *Advances in Neural Information Processing Systems*, 35:23593–23606, 2022. 2, 3, 4
- [19] Diederik P Kingma and Max Welling. Auto-encoding variational bayes. *arXiv preprint arXiv:1312.6114*, 2013. 2
- [20] Suhyeon Lee, Hyungjin Chung, Minyoung Park, Jonghyuk Park, Wi-Sun Ryu, and Jong Chul Ye. Improving 3d imaging with pre-trained perpendicular 2d diffusion models. *arXiv preprint arXiv:2303.08440*, 2023. 3
- [21] Brian Lester, Rami Al-Rfou, and Noah Constant. The power of scale for parameter-efficient prompt tuning. *arXiv preprint arXiv:2104.08691*, 2021. 3
- [22] Ilya Loshchilov and Frank Hutter. Decoupled weight decay regularization. *arXiv preprint arXiv:1711.05101*, 2017. 5
- [23] Ziwei Luo, Fredrik K Gustafsson, Zheng Zhao, Jens Sjölund, and Thomas B Schön. Controlling vision-language models for universal image restoration. *arXiv preprint arXiv:2310.01018*, 2023. 7
- [24] Morteza Mardani, Jiaming Song, Jan Kautz, and Arash Vahdat. A variational perspective on solving inverse problems with diffusion models. *arXiv preprint arXiv:2305.04391*, 2023. 2, 3
- [25] Alec Radford, Jong Wook Kim, Chris Hallacy, Aditya Ramesh, Gabriel Goh, Sandhini Agarwal, Girish Sastry, Amanda Askell, Pamela Mishkin, Jack Clark, et al. Learning transferable visual models from natural language supervision. In *International conference on machine learning*, pages 8748–8763. PMLR, 2021. 3
- [26] Yaniv Romano, Michael Elad, and Peyman Milanfar. The little engine that could: Regularization by denoising (red). *SIAM Journal on Imaging Sciences*, 10(4):1804–1844, 2017. 2
- [27] Robin Rombach, Andreas Blattmann, Dominik Lorenz, Patrick Esser, and Björn Ommer. High-resolution image synthesis with latent diffusion models. In *Proceedings of the IEEE/CVF conference on computer vision and pattern recognition*, pages 10684–10695, 2022. 2
- [28] Olaf Ronneberger, Philipp Fischer, and Thomas Brox. U-net: Convolutional networks for biomedical image segmentation. In *Medical Image Computing and Computer-Assisted Intervention—MICCAI 2015: 18th International Conference, Munich, Germany, October 5-9, 2015, Proceedings, Part III 18*, pages 234–241. Springer, 2015. 2
- [29] Litu Rout, Negin Raoof, Giannis Daras, Constantine Caramanis, Alexandros G Dimakis, and Sanjay Shakkottai. Solving linear inverse problems provably via posterior sampling with latent diffusion models. *arXiv preprint arXiv:2307.00619*, 2023. 3, 5
- [30] Jascha Sohl-Dickstein, Eric Weiss, Niru Maheswaranathan, and Surya Ganguli. Deep unsupervised learning using

- nonequilibrium thermodynamics. In *International conference on machine learning*, pages 2256–2265. PMLR, 2015. [2](#)
- [31] Bowen Song, Soo Min Kwon, Zecheng Zhang, Xinyu Hu, Qing Qu, and Liyue Shen. Solving inverse problems with latent diffusion models via hard data consistency. *arXiv preprint arXiv:2307.08123*, 2023. [3](#)
- [32] Jiaming Song, Chenlin Meng, and Stefano Ermon. Denoising diffusion implicit models. *arXiv preprint arXiv:2010.02502*, 2020. [2](#), [4](#)
- [33] Jiaming Song, Arash Vahdat, Morteza Mardani, and Jan Kautz. Pseudoinverse-guided diffusion models for inverse problems. In *International Conference on Learning Representations*, 2022. [3](#), [4](#)
- [34] Yang Song, Jascha Sohl-Dickstein, Diederik P Kingma, Abhishek Kumar, Stefano Ermon, and Ben Poole. Score-based generative modeling through stochastic differential equations. *arXiv preprint arXiv:2011.13456*, 2020. [2](#), [3](#)
- [35] Narek Tumanyan, Michal Geyer, Shai Bagon, and Tali Dekel. Plug-and-play diffusion features for text-driven image-to-image translation. In *Proceedings of the IEEE/CVF Conference on Computer Vision and Pattern Recognition*, pages 1921–1930, 2023. [5](#), [6](#)
- [36] Singanallur V Venkatakrishnan, Charles A Bouman, and Brendt Wohlberg. Plug-and-play priors for model based reconstruction. In *2013 IEEE global conference on signal and information processing*, pages 945–948. IEEE, 2013. [2](#)
- [37] Yinhuai Wang, Jiwen Yu, and Jian Zhang. Zero-shot image restoration using denoising diffusion null-space model. *arXiv preprint arXiv:2212.00490*, 2022. [2](#), [3](#), [4](#)

Regularization by Texts for Latent Diffusion Inverse Solvers

Supplementary Material

8. Implementation Details

In this section, we provide further details on implementation of *TReg*. The code will be available to public on <https://github.com/TReg-inverse/Treg>.

8.1. Stable-diffusion and CLIP

We leverage the pre-trained Latent Diffusion Model (LDM), including an auto-encoder and the U-net model, provided by diffusers. Due to the limitation of its modularity, we implement the sampling process for inverse problems by ourselves, rather than changing given pipelines. The Stable-diffusion v1.5 is utilized for every experiment in this work, and the ViT-L/14 backbone is used for CLIP image encoder for adaptive negation.

8.2. DDIM Sampling

For the DDIM sampling following the data consistency update, the general form of update rule is described as

$$\mathbf{z}'_{t-1} = \sqrt{\bar{\alpha}_{t-1}}\hat{\mathbf{z}}_0 + \sqrt{1 - \bar{\alpha}_{t-1}}\tilde{\epsilon}_t, \quad (19)$$

where $\hat{\mathbf{z}}_0$ is the *denoised* estimate and $\tilde{\epsilon}_t$ denotes the total noise. The total noise is given by

$$\tilde{\epsilon}_t := \frac{\sqrt{1 - \bar{\alpha}_{t-1} - \eta^2 \tilde{\beta}_t^2 \hat{\epsilon}_\theta + \eta \tilde{\beta}_t \epsilon}}{\sqrt{1 - \bar{\alpha}_{t-1}}}, \quad (20)$$

where $\eta \tilde{\beta}_t$ is a hyper-parameter that controls the stochasticity of the update. In this work, we set $\eta \tilde{\beta}_t = \sqrt{\bar{\alpha}_{t-1}(1 - \bar{\alpha}_{t-1})}$ so that the (20) becomes

$$\tilde{\epsilon}_t = \sqrt{1 - \bar{\alpha}_{t-1}}\hat{\epsilon}_\theta + \sqrt{\bar{\alpha}_{t-1}}\epsilon. \quad (21)$$

Here, the data consistency update is applied for a subset of sampling steps, as described by Γ in Algorithm 1 of the main paper. Our empirical observation show that this partial data consistency update achieves better trade-off between the image reconstruction consistency and the latent stability. In the absence of the data consistency update, we employ the deterministic DDIM sampling step by setting $\eta \tilde{\beta}_t = 0$. Overall, for all inverse problems in this work, we set the Network Function Evaluation (NFE) to 200 and design $\Gamma = \{t | t \bmod 3 = 0, t \leq 850\}$ ³, where mod denotes the modulo operation.

³The pre-trained Stable-diffusion uses $T = 1000$. Thus, $t = 850$ is equivalent to the sampling step with $\text{NFE} = 170$.

8.3. CFG guidance scale

The classifier-free guidance (CFG) is defined as

$$\hat{\epsilon}_\theta = \epsilon_\theta(\mathbf{z}_t, \phi, t) + \omega(\epsilon_\theta(\mathbf{z}_t, \mathbf{c}, t) - \epsilon_\theta(\mathbf{z}_t, \phi, t)) \quad (22)$$

where ω is a scale for the guidance. In other words, ω could be interpreted as a magnitude for the negation. Thus, we leverage ω to control the extent of enhancement applied to a given text prompt. In fact, we can regulate the same feature by adjusting the null-text update strategy, including null-text update frequency and number of optimization iterations per time step. However, the CFG guidance scale is simpler and more intuitive than adjusting the null-text update strategy. Hence, we have used a proper CFG scale while fixing the null-text update schedule Γ .

For the main experiments with the Food101 dataset in the main paper, we use the default scale 7.5 for all results. For other results, including the extended results in the appendix, CFG scale among $\{3.0, 4.0, 5.0, 7.5\}$ provide robust performance for various datasets including FFHQ, AFHQ LHQ, and ImageNet.

8.4. Conjugate gradient method

In this work, we apply the CG method to find a solution to the following problem:

$$\min_{\mathbf{x}} \frac{\|\mathbf{y} - \mathcal{A}\mathbf{x}\|_2^2}{2\sigma^2} + \lambda \|\mathbf{x} - \mathcal{D}_\varphi(\hat{\mathbf{z}}_{0|t})\|_2^2. \quad (23)$$

As the objective function is a convex function, the solution \mathbf{x}^* should satisfy

$$-\mathcal{A}^\top(\mathbf{y} - \mathcal{A}\mathbf{x}^*) + \lambda(\mathbf{x}^* - \mathcal{D}_\varphi(\hat{\mathbf{z}}_{0|t})) = 0, \quad (24)$$

where the coefficients are absorbed to λ . Then, we can formulate it as a linear system as

$$(\lambda \mathbf{I} + \mathcal{A}^\top \mathcal{A})\mathbf{x}^* = \lambda \mathcal{D}_\varphi(\hat{\mathbf{z}}_{0|t}) + \mathcal{A}^\top \mathbf{y} \quad (25)$$

where $\mathbf{A} = \lambda \mathbf{I} + \mathcal{A}^\top \mathcal{A}$ and $\mathbf{b} = \lambda \mathcal{D}_\varphi(\hat{\mathbf{z}}_{0|t}) + \mathcal{A}^\top \mathbf{y}$. Thus, we can solve (25) by CG method. In this work, we use 5 iterations of CG update with $\lambda = 1e - 4$ for each time step.

9. Ablation study

9.1. Effectiveness of adaptive negation

In this work, we propose a novel concept of the adaptive negation, a method designed to optimize the null-text to minimize similarity with the current denoised estimation in the CLIP embedding space. This approach aims

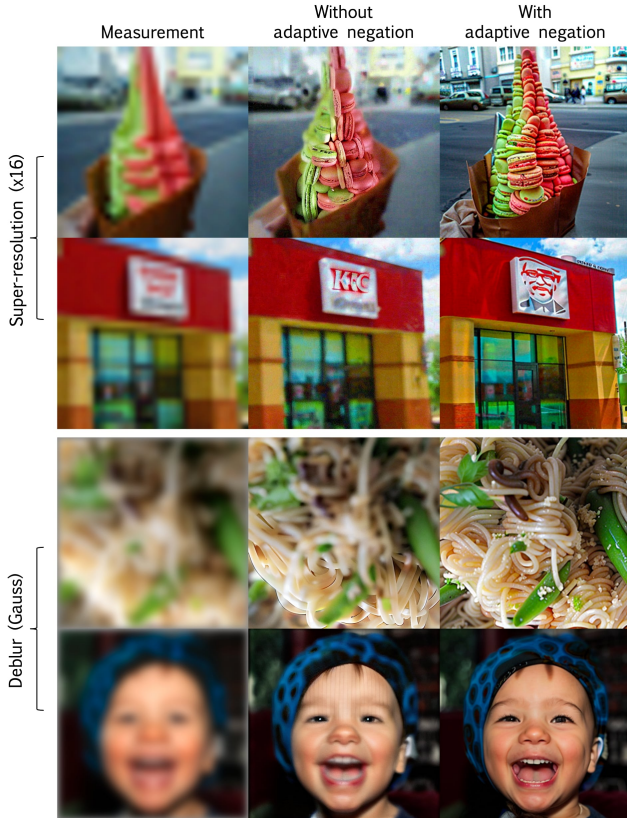


Figure 7. Comparison of reconstruction results with and without the adaptive negation.

to enhance the text guidance by suppressing complementary concepts through concept negation in CFG. To investigate the efficiency of the adaptive negation, we conduct an ablation study. Figure 7 compares reconstructed images with and without the adaptive negation for super-resolution and deblur tasks using representative examples from various datasets. In all cases, adaptive negation effectively enhances the given textual conditions, ensuring that the reconstructed image contains the intended concept more clearly. Furthermore, the results reveal that the adaptive negation not only enhances the text guidance but also improves the overall quality of reconstruction. This is because complementary concepts may include prompts related to the image quality. For instance, negative prompts like “*blurry*” and “*out of focus*” are commonly used to enhance the fidelity of generated images in practice. We believe that the proposed adaptive negation achieves a similar effect through optimization without any human-originated prompt engineering, supporting the effectiveness of the method.

10. Additional Results

10.1. Box Inpainting

Due to the page limitation, we only provide the results for two inverse problems; super-resolution and deblurring. However, we can apply $TReg$ to another challenging linear inverse problem, inpainting. We use the same settings as other problems. To avoid the boundary effect and improve the consistency of the masked region, we utilize the DPS step for $t \notin \Gamma$. To assess the efficiency of the proposed method across diverse domains, we select the AFHQ and FFHQ datasets for our analysis. In the case of both AFHQ and FFHQ, our intention is to employ a universal mask that encompasses the eyes and mouth. To achieve this, we generate a box mask based on averaged images across all data points within each dataset. Figure 8 and 9 show that the proposed method can solve the inpainting problem with high-quality reconstruction results. Specifically, for both dogs and cats, the proposed method fills out masked regions by reflecting the given prompt. Also, in Figure 10, the proposed method exhibits its capability to solve the inpainting problem with the composition of concepts. In other words, $TReg$ has the capability to narrow down the solution space, by utilizing not only a singular concept but also multiple concepts simultaneously.

10.2. Super-resolution and Deblurring

In this section, we provide extended results for measurements to support the efficiency and compatibility of the proposed $TReg$ with various domains. Specifically, we leverage the proposed method for super-resolution and deblurring tasks on FFHQ, LHQ (high-resolution landscape image dataset), and Food101. For FFHQ, we examine the reconstruction with text prompts “*baby face*” and “*adult face*”. As shown in Figure 11 and 12, the proposed method successfully reconstructs images according to the given prompt, while the baseline method (sequential approach of PSLD and DDS) shows inferior reconstruction quality. For LHQ, we examine the reconstruction with text prompts related to the style of images, including “*photography*”, “*Monet*”, and “*watercolor*”. Note that, in contrast to the FFHQ or AFHQ datasets, the landscape images contain more diverse and detailed structures, making the inverse problems inherently more challenging. Figure 13 and 14 demonstrate the effectiveness of the proposed method, even for handling challenging problems. The method retains fidelity to the text prompt while maintaining data consistency with the provided measurement. Following Figure 15 and 16 illustrate extended results on the Food-101 dataset. As with other results, the proposed method allows us to reconstruct images with diverse concepts by preserving data consistency.



Figure 8. Representative results for inpainting task on AFHQ (dog) dataset. With TReg, we can precisely control the content of the hidden region to our intention.



Figure 9. Representative results for inpainting task on AFHQ (cat) dataset. With TReg, we can precisely control the content of the hidden region to our intention.

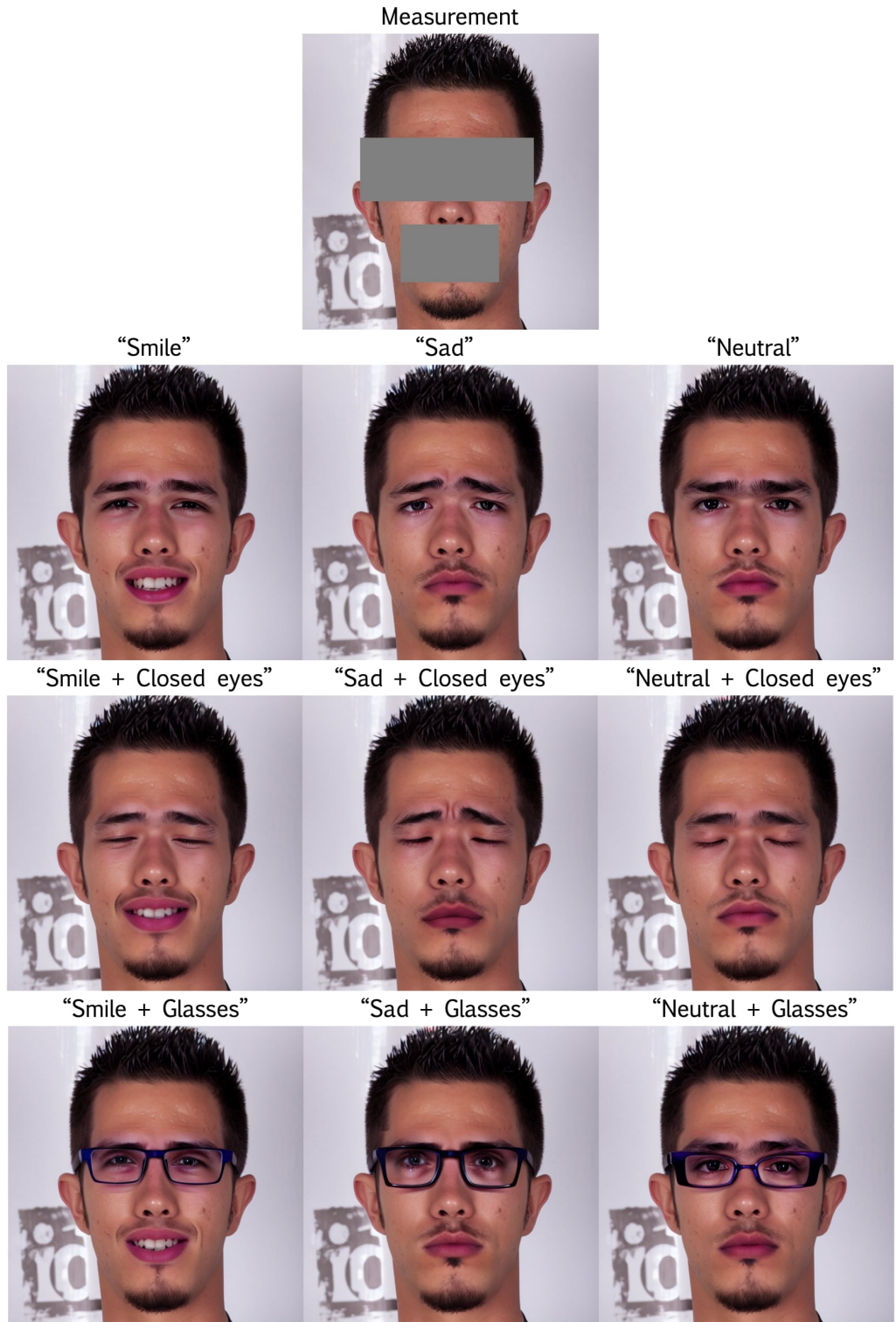


Figure 10. Reconstructed results for inpainting task on human face with various compositional text prompts.

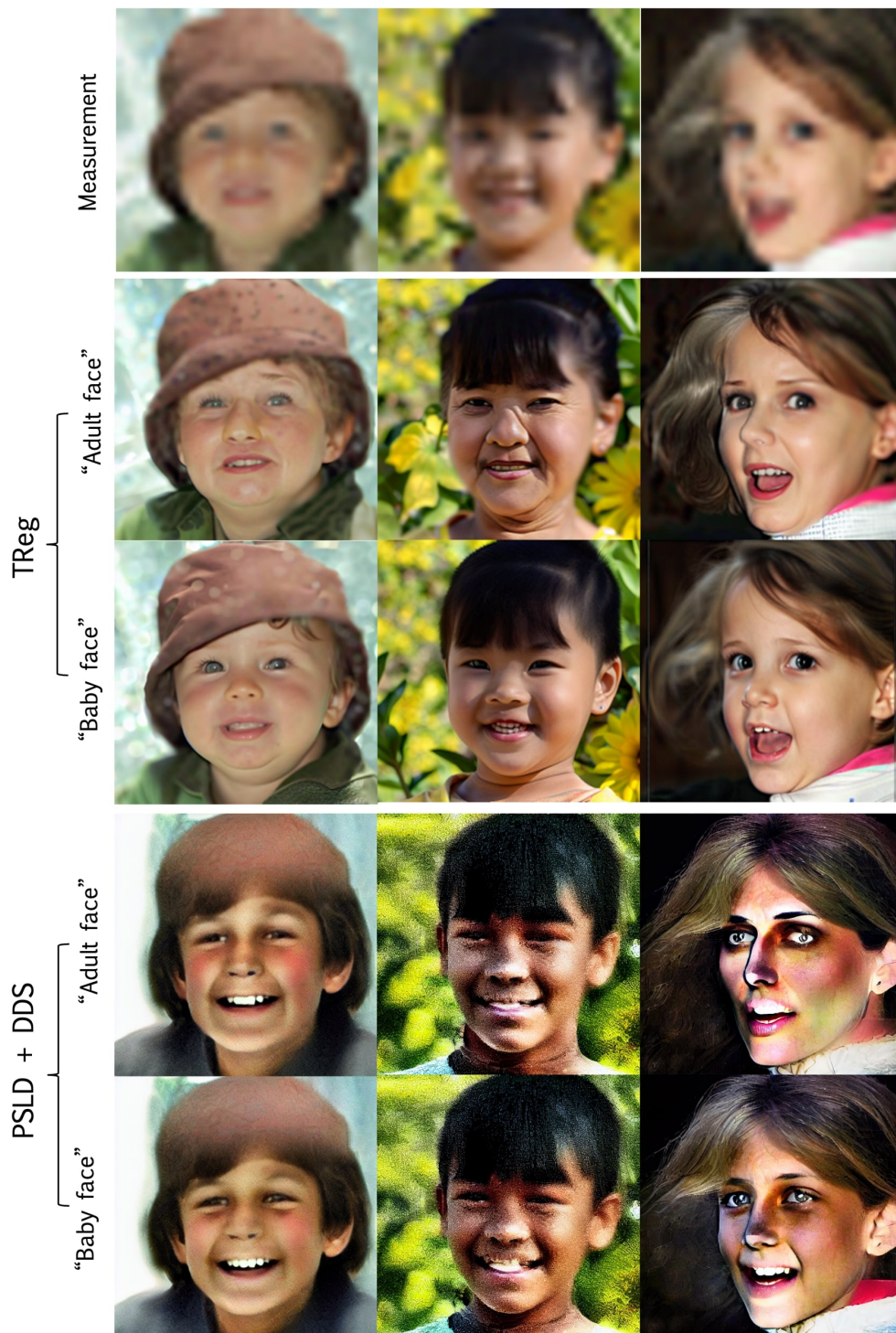


Figure 11. Reconstruction result for SR (x16) task on FFHQ dataset. Our method outperforms the existing methods (PSLD+DDS) in terms of the reconstruction quality.



Figure 12. Reconstruction result for Deblur (Gaussian blur) task on FFHQ dataset. Our method outperforms the existing methods (PSLD+DDS) in terms of the reconstruction quality.

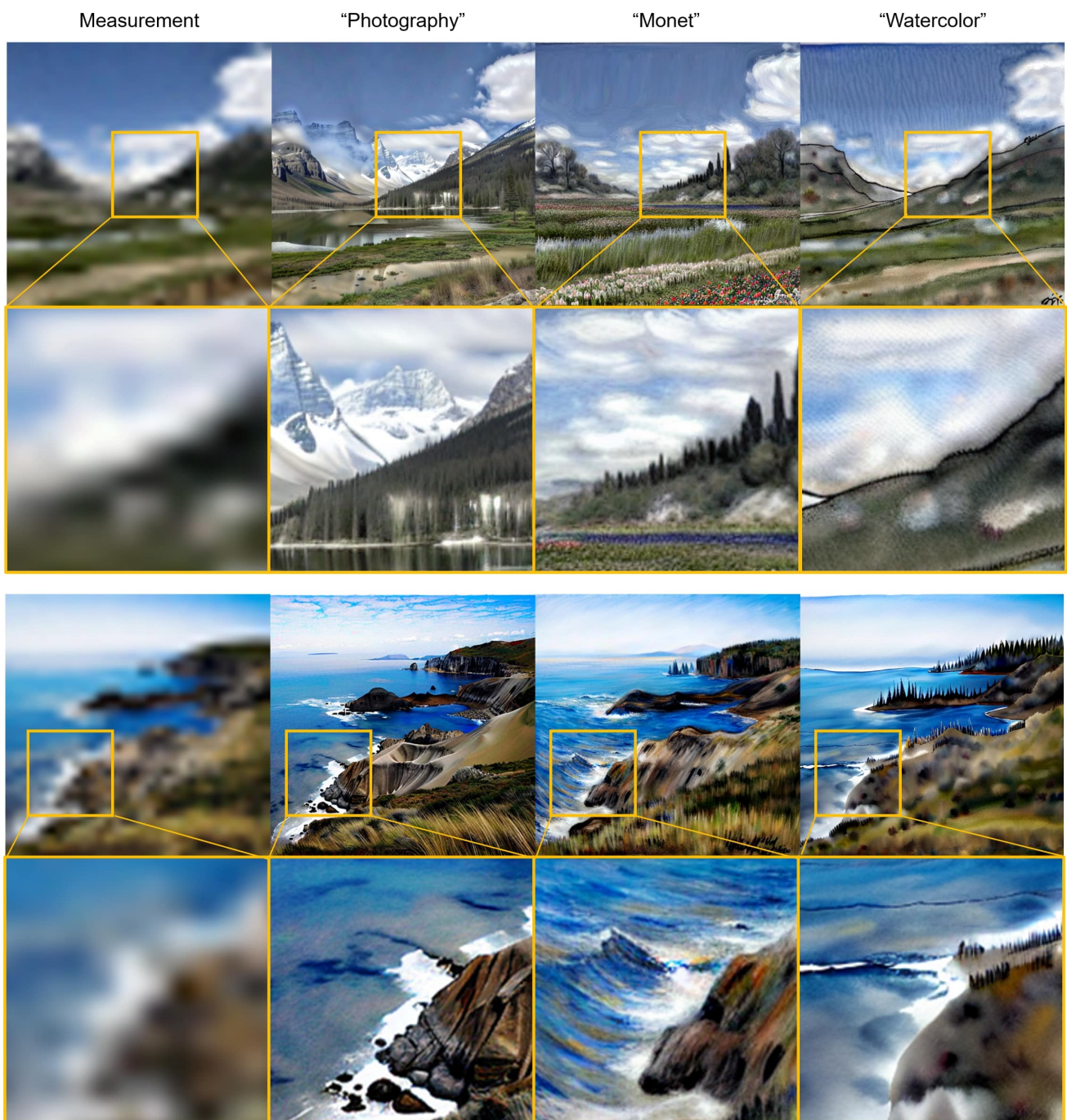


Figure 13. Reconstruction result for SR(x16) task on LHQ dataset. Enlarged views correspond to yellow rectangles in the upper view.

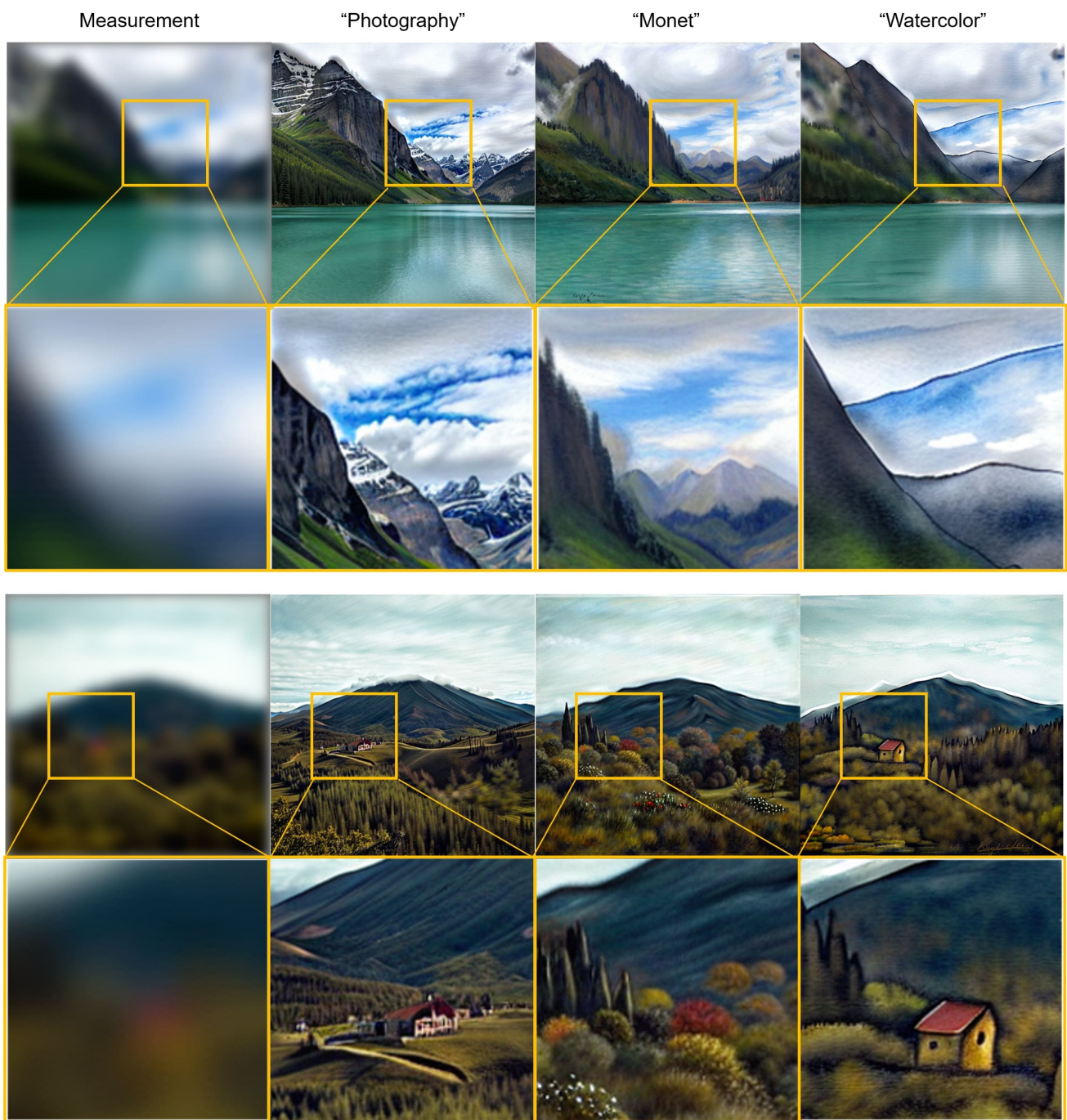


Figure 14. Reconstruction result for Deblur (Gaussian blur) task on LHQ dataset. Enlarged views correspond to yellow rectangles in the upper view.



Figure 15. Reconstruction results with diverse prompts for SR (x16) task on Food dataset. Our methods has precise control of the reconstruction that matches our intention and measurement.



Figure 16. Reconstruction results with diverse prompts for Deblur (Gaussian) task on Food dataset. Our methods has precise control of the reconstruction that matches our intention and measurement.